ELSEVIER

Journal of Power Sources 59 (1996) 63–69

JOURNAL OF POWER SOURCES

# Microstructure and properties of continuously cast, lead-alloy strip for lead/acid battery grids

N.-Y. Tang, E.M.L. Valeriote, J. Sklarchuk

*Cominco Ltd., Product Technology Centre, Sheridan Park, Mississauga, Ont., L5K 1B4, Canada*

Received 15 November 1995; accepted 8 December 1995

**Abstract**

Lead/acid battery grid alloys, such as low-antimony–lead and lead–calcium–tin alloys with and without silver, are successfully continuously cast into strip using Cominco's Multi-Alloy Caster™. The mechanical and electrochemical properties of the continuously cast, low-antimony–lead strip are strongly dependent on the arsenic content in the alloys. On the other hand, the tin:calcium (Sn:Ca) ratio in the Pb–Ca–Sn alloys plays an important role in the development of the microstructure and the mechanical properties of these alloys.

*Keywords:* Lead/acid batteries; Grid alloy; Casting; Lead; Calcium

## 1. Introduction

To reduce water-maintenance requirements, the antimony content in commercial grid alloys for starting-lighting-ignition (SLI) batteries has been lowered by many battery manufacturers to less than 2 wt.%. To maintain adequate performance and service life, the popular composition at present contains between 1.6 and 2 wt.% of antimony. Due to solute redistribution during solidification, the freezing range of such low-antimony–lead alloys is well over 60 °C. Consequently, the alloys are difficult to cast, either continuously or by conventional methods. Grain refiners (such as selenium, sulfur and copper) are added to aid gravity casting of battery grids [1–3].

Another grid alloy that has been developed successfully in recent years is a lead–calcium–tin–silver alloy [4]. The silver addition is found to improve the corrosion resistance of the alloy and, thereby, improves the overall performance of the batteries. During solidification of the alloy, however, silver is found to be enriched in the unsolidified inter-dendritic portion which, finally, forms a eutectic. Consequently, such an alloy has a freezing range of about 20 °C [5], and is impossible to continuously cast using a dip-caster [6,7].

Over the last two to three decades, there has been a constant effort to develop a continuous, automated, processing technology for lead/acid battery grid alloys for positive plates [8–10]. One route, in which strip was produced by rolling, was explored for low-antimony–lead alloys without success. Its ill fate can be attributed to inadequate creep strength of the wrought strip, which led to excessive growth of the positive plates and, consequently, to a short battery life [9]. Another route was to produce the strip by a continuous casting process. As mentioned earlier, however, low-antimony–lead alloys and lead–calcium–tin alloys with silver additions solidify over wide temperature ranges. Consequently, these alloys are susceptible to hot shortness in casting.

After overcoming a number of technical difficulties, Cominco has successfully developed a caster based on the melt-drag process. This Multi-Alloy Caster™ is capable of casting a number of lead alloys and makes possible a complete, continuous, battery grid-processing technology. This is based on continuous expansion by rotary tools of continuously drum-cast, lead-alloy strip. In general, a complete production line consists of a caster, a rotary expander, and other mesh and plate-processing machinery. This automated plate-manufacturing process has been well accepted by manufacturers of lead/acid batteries, because of its cost-effective speed and material and labour utilization. Currently, there are more than 24 casters (including five Multi-Alloy Casters™) and more than 35 expanders being used in production in more than 13 battery manufacturing plants around the world.

Due to the high cooling rate achieved on the Multi-Alloy Caster™ during solidification, grain refiners are not essential; the homogeneity of alloy element distribution and the soundness of the cast structure have been improved considerably. Consequently, the mechanical strength and corrosion resistance of the alloys have also been enhanced. The electrochemical performance of battery grids fabricated from cast,


*SSDI* 0378-7753(95)02303-8

low-antimony–lead strip has been discussed previously [11]. Information on the microstructure and properties of these drum-cast alloys is reported here.

## 2. Experimental

The sample strips investigated in this study were all continuously cast using Cominco's Multi Alloy Caster™. The casting drum was made of aluminum alloy, whose internal surface was constantly cooled by circulating water, with temperatures maintained between 40 and 45 °C.

Specimens for metallurgical examination were cold-mounted using a mixture of 2 parts by volume of Buehler No. 20-3552 plastic powder and 1 part of No. 20-3554 plastic liquid. The specimens were allowed to cure at ambient temperature for at least 4 h. They were then successively ground on progressively finer emery paper down to 600 grit, followed by mechanical polishing on microcloth using 0.3 μm alumina powder. The specimens were subsequently chemically polished and etched by swabbing for about 15 s with a solution of 3 parts (by volume) of glacial acetic acid and 1 part of hydrogen peroxide. To reveal clearly cell and grain boundaries, the specimens were further swabbed with a solution of 9 g ammonium molybdate and 15 g citric acid in 90 ml of distilled water.

Scanning electron microscopy (SEM) was carried out using an ETEC Autoscan equipped with a Kevex EDS unit.

Creep tests were carried out using dead-weight rigs. The details of the creep tests have been given elsewhere [12]. Experimental details for electrochemical tests have also been reported previously [11].

## 3. Results and discussion

### 3.1. Microstructure

The melt-drag process produces strip with microstructures that are free of visible casting defects. The structures differ in detail due to variation in alloy composition and casting conditions. In general, the grain structure of an as-cast, low-antimony–lead strip can be divided into three zones. As shown in Fig. 1(a), the surface which is either exposed to air or in direct contact with the casting drum during casting consists of equiaxial fine grains. Between the surface zones are well-developed columnar grains with their axes approximately perpendicular to the strip surface, the main heat-flow direction. The dimension of the equiaxial grain zone at its top (air) surface varies with the strip thickness: the thicker the strip, the thicker the zone. The cells within the grains can be clearly revealed. For Pb–Ca–Sn alloys, the cells are generally less well defined, as shown in Fig. 1(b). Also, the fine equiaxial grains in the near surface layers are not always well developed. The microstructure of these two types of alloy are described further in the following sections.

#### 3.1.1. Pb–Sb–As–Sn

The grain structures in the middle zones of a number of low-antimony–lead alloys cast under similar conditions are shown in Fig. 2(a)–(d). This set of micrographs indicates that both selenium and arsenic are effective grain refiners, especially when these two elements are added together. With the addition of selenium, a significant modification in the grain structure was also noticed. The grains became finer, and the shape of grains in the middle zone changed from columnar to equiaxial. Practice indicated that, for the melt-drag casting process, the addition of grain refiners was not essential, as shown in Fig. 2(a) and (b). Pb–Sb binary and Pb–Sb–Sn ternary alloy, without any grain refiners, could be cast with ease.

The microstructure of such alloys consisted mainly of two constituents: a lead-rich solid solution with an embedded fine dispersion of precipitates (that can only be resolved by SEM), and a small fraction of degenerated eutectic that formed at the cell and grain boundaries. The grain structure of the drum-cast strip should be compared with that of grav-

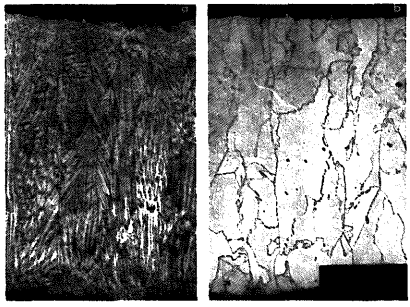

Fig. 1. Typical grain structure of strip produced by a melt-drag process: (a) Pb–1.7Sb–0.12As–0.1Sn, and (b) Pb–0.09Ca–0.8Sn.

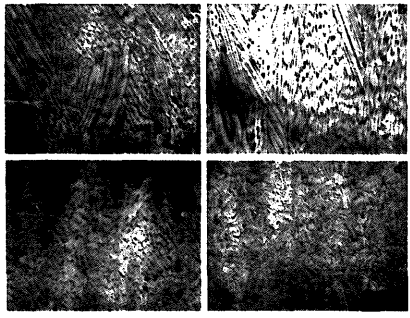

Fig. 2. Grain structure of low-antimony–lead alloys produced by melt-drag process: (a) Pb–1.5Sb; (b) Pb–1.5Sb–0.22Sn; (c) Pb–1.5Sb–0.22Sn–0.13As, and (d) Pb–1.5Sb–0.22Sn–0.13As–0.04Se.

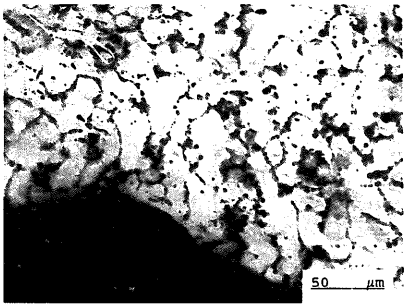


Fig. 3. Grain structure of a book-mould cast grid containing 1.6 wt.%Sb. Antimony precipitates are coarse and their volume fraction is higher than that in a melt-drag strip with the same composition.

ity-cast, book-mould grids of comparable composition. As shown in Fig. 3, the antimony precipitates in a comparable book-mould grid were coarser, and casting defects (such as gas pores and shrinkage pores) were frequently found.

### *3.1.2. Pb–Ca–Sn and Pb–Ca–Sn–Ag*

The grain structure of these alloys produced on the Multi-Alloy Caster™ are largely dependent on the Sn:Ca ratio in the alloys. At a weight ratio around 3, the grains were intertwined and the grain boundaries were wavy due to discontinuous precipitation. With a ratio higher than 10, the discontinuous precipitation process was substantially delayed, and even totally suppressed, as can be seen in Fig. 1(b). With the addition of approximately 0.03 wt.% Ag, the microstructure was not noticeably modified. Nevertheless, the cells within grains were all well developed.

## 4. Mechanical properties

Arsenic was found to have a strong effect on the mechanical properties, including both the tensile and creep strength of low-antimony–lead strip. The mechanical properties of the Pb–Ca–Sn alloys were largely dependent on the Sn:Ca ratio and, to a lesser degree, on the amount of tin in solid solution in the alloy.

### *4.1. Tensile properties*

The ultimate tensile strength of a typical low-antimony–lead alloy containing 1.7 wt.% Sb, 0.15 wt.% As and 0.2 wt.% Sn (Pb–1.7Sb–0.15As–0.2Sn) is approximately 35 MPa. A solution treatment followed by water quenching could increase the tensile strength to 70 MPa.

The age-hardening behaviour of the low-antimony–lead alloys was largely dependent on the arsenic content. Alloys without arsenic addition were rather soft immediately after being cast, and aged at an extremely slow rate. In general, low-antimony–lead alloys aged quickly at room temperature; however, overageing did not occur even after more than one year. The increase in hardness of a Pb–1.5Sb–0.1As–0.2Sn–0.02Se alloy due to natural ageing is shown in Fig. 4.

The evolution of the tensile strength of cast Pb–Ca–Sn alloy strip was largely dependent on the Sn:Ca ratio. For this type of alloy, the cooling rates realized on a dip caster [13] and a Multi-Alloy Caster™ were similar, and the ageing behaviours of the alloys cast on these two types of caster were found to be similar. The evolution of tensile strength of Pb–Ca–Sn alloys cast on a dip-caster due to natural ageing is shown in Fig. 5 [13]. When the ratio is low, the alloy is strengthened through a rapid discontinuous precipitation process [14–16]. For example, a Pb–0.09Ca–0.3Sn alloy gains about 85 to 90% of its attainable strength within less than 1 h after casting. Also, the initial strength of the alloys appears to be inversely related to their tin content, a phenomenon that is not fully understood at this stage. In general, the tensile properties, including yield strength and ultimate ten-

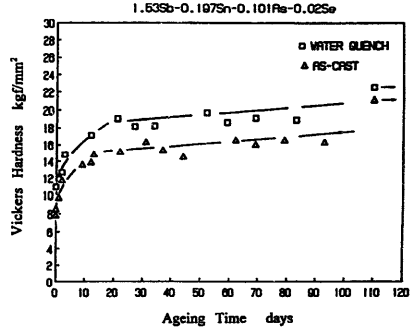


Fig. 4. Natural ageing of low-antimonial-lead alloy at room temperature. Overageing did not occur after more than one year. Solution treatment, followed by water quenching, increased the hardness of the alloy.

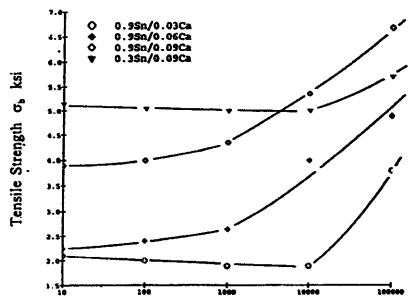


Fig. 5. Natural ageing of Pb–Ca–Sn alloys.

sile strength of the cast Pb–Ca–Sn alloys, increase with the progress of the natural ageing process.

The ageing behaviour of Pb–Ca–Sn–Ag alloy was similar to its silver-free counterpart.

### 4.2. Creep strength

Creep behaviour of the cast strip was studied extensively. Some of the creep tests were carried out shortly after the strip was cast, and some were carried out after the strip was stored at room temperature for more than two years when all the alloys were fully naturally aged.

Typical creep curves for the cast strip are shown in Fig. 6. The creep of a low-antimony–lead alloy can be divided into three stages: (i) a protracted primary transient; (ii) a steady-state in which the creep rate was approximately constant, and (iii) a tertiary stage (not shown in Fig. 6) in which the creep accelerated due to extensive structural damage developed in the test piece. On the other hand, the creep behaviour of the Pb–Ca alloys was peculiar. Frequently, there was no well-defined steady state. The creep accelerated after the primary creep stage, and the alloy revealed a strain-softening behaviour.

To gain some insight into the mechanism at work, creep rates were measured over a range of stress from 5 to 10 MPa. The strain-rate/stress curves for the two types of alloy are given in Fig. 7. It can be seen that the data in the log–log plot fell into straight lines with a slope of about 4. This signifies that, within the stress range investigated, lead alloys underwent power-law creep, in which dislocation climb was the rate-limiting process. One important observation is that the creep strength of low-antimony–lead alloys was generally higher than that of Pb–Ca–Sn alloys. The creep rates of low-antimony–lead alloys were found to be overwhelmingly

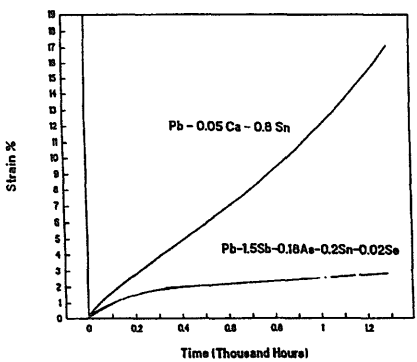


Fig. 6. Typical creep curves for lead alloys produced by melt-drag process. Pb–Ca–Sn alloys frequently revealed strain softening in creep. Test carried out at 70 °C and 6 MPa. Test of low-antimony–lead strip was interrupted due to time restraint.

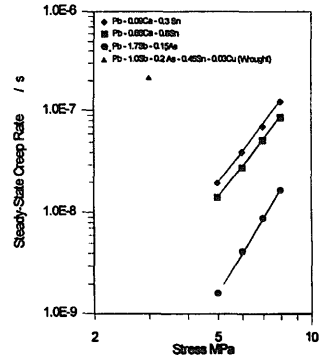


Fig. 7. Strain rate-stress relationship in creep of lead alloys. Within the stress range under study, the dominant deformation mechanism is dislocation creep.

determined by the arsenic content, $C_{As}$ in wt.%, in the alloys. Regression analysis indicated that, at MPa and 70 °C, the steady-state creep rate of the alloys, $\dot{\epsilon}$, was an exponential function of arsenic content:

$$\dot{\epsilon} = 2.23 \exp(-11.7 C_{As}) \times 10^{-8}\ s^{-1} \quad r^2 = 0.9956 \qquad (1)$$

The above equation was applicable for an arsenic content up to about 0.2 wt.%. Further increase in arsenic content resulted in deterioration in the creep resistance of the alloy. Microstructural examination indicated that the grain size of alloys with a high arsenic content became extremely small. It is well established that grain-boundary sliding becomes an important creep mechanism for materials with a small grain size.

The creep resistance of melt-drag, low-antimony–lead strip was much higher than wrought strip with a similar composition. The steady-state creep rate of wrought strip containing 0.2 wt.% As at 70 °C and 3 MPa is also shown in Fig. 7. The creep rate of the as-wrought strip was over two orders of magnitude higher than that of the cast strip of similar composition. It was found that the creep strength of a wrought strip can be substantially improved by an annealing treatment. After being annealed at 245 °C for 1 h, the creep rate of the wrought strip decreased by over one order of magnitude. Nevertheless, the creep rate of the wrought low-antimony–lead strip after annealing was still about one order of magnitude higher than that of cast strip. By a thermo-mechanical treatment, the tensile strength, especially the yield strength, of wrought strip could be improved substantially due to a high dislocation density introduced during the treatment. Dislocation cores, however, are easy diffusion paths. Consequently, diffusion processes were substantially enhanced. Wrought strip is known for its inferior growth characteristics from laboratory tests [9]. This is a clear indication that grid growth is a creep process, which cannot be judged based on

Table 1
Minimum creep rates of Pb–Ca–Sn alloys at 70 °C and 6 MPa

| Alloy | Composition (wt.%) | Minimum creep rate ($10^{-8}$/s) | | Observation |
|---|---|---|---|---|
| | | Under aged | Fully aged | |
| 112692 | Pb–0.075Ca–0.93Sn | 4.3 | 2.1 | softening |
| 112792 | Pb–0.050Ca–0.88Sn | 3.2 | 3.2 | softening |
| 120192A | Pb–0.045Ca–0.98Sn | 3.8 | 3.1 | hardening |
| 120192B | Pb–0.055Ca–0.98Sn | 3.4 | n.a. [a] | hardening |
| 120292 | Pb–0.060Ca–0.84Sn | 2.4 | 2.0 | hardening |
| 120392 | Pb–0.078Ca–1.06Sn | 4.3 | 4.4 | softening |
| 120492 | Pb–0.084Ca–1.07Sn | 5.2 | n.a. | softening |
| 120792 | Pb–0.085Ca–0.81Sn | 4.7 | n.a. | n.a. |
| 121492 | Pb–0.092Ca–0.76Sn | 6.6 | 6.7 | softening |
| 121592 | Pb–0.116Ca–0.76Sn | 11.6 | 8.9 | softening |
| 903 | Pb–0.09Ca–0.3Sn | n.a. | 4.2 | softening |

[a] n.a.: information not available.

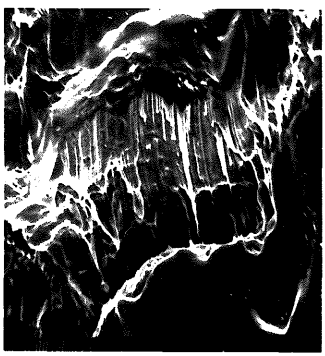

Fig. 8. Creep fracture morphology of Pb–0.09Ca–0.3Sn alloy. Strain softening in creep led to grain fragmentation.

the tensile properties of an alloy. Due to its poor creep performance, wrought antimonial strip would appear to be inadequate for application in automotive (SLI) batteries.

The minimum creep rates of a number of Pb–Ca–Sn alloys, tested at 70 °C and 6 MPa, are listed in Table 1. A preliminary analysis of the data indicates that the creep strength of the cast strip was inversely related to the calcium content in the alloys. Natural ageing for over two years did not noticeably improve creep strength. Also, most alloys showed strain softening rather than hardening. The fracture morphology of the creep specimens that showed strain softening is shown in Fig. 8. It can be seen that a large number of localized deformation bands were formed during the test at 70 °C and 6 MPa. These resulted in grain fragmentation in addition to the normal intergranular cavitation. Strain softening in Pb–Ca alloys has been well studied [14]. Nevertheless, an understanding of the inverse relation between creep strength and calcium content is still being awaited. The precipitation of $(PbSn)_3Ca$ was studied by Bouirden et al. [15] using transmission electron microscopy (TEM). They found that the precipitation mechanism changed with the Sn:Ca weight ratio. When the ratio was less than 3, three successive discontinuous precipitation reactions took place in the alloy. Discontinuous precipitation was totally suppressed in alloys with an Sn:Ca ratio higher than 9. Alloys with an intermediate Sn:Ca ratio exhibited a mixed-precipitation behaviour; a continuous precipitation reaction took place after two discontinuous precipitation reactions. Particles formed in the first two discontinuous precipitation processes were found to be coherent and ordered, with a dimension about 10 nm. These densely distributed fine particles strengthen the lead matrix mainly through order hardening. Dislocations can only travel in the matrix through shearing these $(PbSn)_3Ca$ particles. After being scrambled by the dislocations, these particles lose their order and are no longer effective in strengthening the matrix. Consequently, this slip band became an easy path for moving dislocations. Some particles in the band would dissolve because their dimension may become smaller than the critical size. Also, dynamic recrystallization would take place in these localized deformation bands [14]. For a given tin content, a high calcium content reduces the Sn:Ca ratio and encourages the discontinuous precipitation of fine $(PbSn)_3Ca$ particles and, thereby, favours the shear mechanism during deformation. The strain-softening phenomenon was suppressed by a high Sn:Ca ratio. It is believed that a mixture of fine particles (due to discontinuous precipitation) and coarse particles [16] precipitated out during the continuous precipitation, changed the particle shear mechanism to a shear plus bypassing mechanism and, accordingly, activated the strain-hardening mechanism.

## 5. Electrochemical properties

As expected, the corrosion resistance of the Pb–Ca–Sn alloy strip was generally higher than that of the Pb–Sb–As–Sn alloy strip, which in turn was better than that of a book-mould cast grid of a similar composition. The weight losses of various lead alloy grids after a 16-day potentiostatic corrosion test are shown in Fig. 9. The weight loss of the silver-containing Pb–Ca–Sn alloy was the lowest, and that of the low-antimony–lead grid cast by the conventional book mould method was the highest, even though its arsenic content was much lower than that in other low-antimony–lead alloys tested in the same cell.

The weight loss of a low-antimony–lead alloy in a constant-potential corrosion test was affected by both the antimony and arsenic contents. A multi-linear regression analysis of results of a number of corrosion tests indicated that the effect of increased arsenic content in increasing the corrosion rate was one order of magnitude stronger than that of antimony. In other words, as far as corrosion is concerned, 0.1 wt.% As is equivalent to 1 wt.% Sb. As shown in Fig. 10, the weight losses of the alloys were a linear function of the anti-

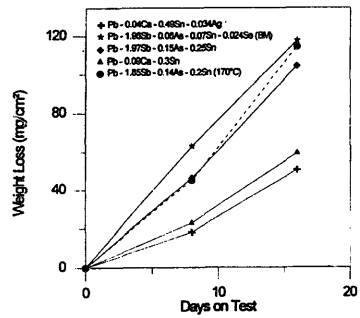


Fig. 9. Weight losses of various lead alloy grids in potentiostatic corrosion tests at 200 mV overpotential and 70 °C. The book-mould grid suffered the highest weight loss, although its arsenic content was the lowest among the three low-antimony–lead alloys.

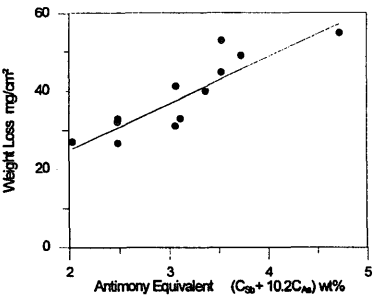


Fig. 10. Weight losses of low-antimony–lead alloy coupons after constant-potential corrosion tests at 150 mV overpotential and 60 °C for 28 days. All strips were heat-treated at 200 °C. Weight loss was a linear function of antimony equivalent defined as ($C_{Sb} + 10.2C_{As}$) and $C_{Sb}$ ranges from 1.5 to 3 wt.%.

Table 2
Test results for positive plates with cast-expanded grids

| Alloy | Weight loss ($mg\ cm^{-2}$) | Area growth (%) | | Thickness ratio |
|---|---|---|---|---|
| | | Measured | Calibrated | |
| Pb–1.50Sb–0.10As | n.a. [a] | 8.0 | 10.9 | 1.36 |
| Pb–1.88Sb–0.12As | 43.3 | 10.7 | 10.7 | 1 |
| Pb–1.43Sb–0.13As | 50.5 | 8.8 | 9.8 | 1.11 |
| Pb–1.97Sb–0.17As | 50.7 | 7.4 | 8.36 | 1.13 |

[a] n.a.: information not available.

mony equivalent defined as ($C_{Sb} + 10.2C_{As}$). The growth rates of positive plates containing expanded low-antimony–lead alloy grids were found to be inversely related to the arsenic contents. The area growths of grids after 23 cycles in a deep-discharge test performed at 71 °C are shown in Table 2. The growth data were calibrated for the thickness differences of the grids by multiplying the raw data, shown in the 'measured' column by the thickness ratio (the thickness of Pb–1.88Sb–0.12As strip was taken as unity). The results are listed in the 'calibrated' column. Such a calibration is necessary because tests indicated that, with test conditions being identical, a thicker strip grew less than a thinner one of the same composition [17]. A regression analysis indicated that the calibrated area growth, $G$, was approximately exponentially related to the arsenic content in the grid alloys, i.e.:

$$G = 16.7 \exp(-4.0C_{As}) \quad r^2 = 0.9750 \qquad (2)$$

where $C_{As}$ has been defined earlier.

The seemingly contradictory effects of arsenic on the electrochemical performance of an alloy can be understood only after a thorough understanding of the growth mechanism is reached. In a recent publication [12], it was demonstrated that the driving force for grid growth was corrosion-induced stress, and that the growth rate was inversely related to the creep resistance of an alloy. Although an increased corrosion rate due to a high arsenic content increases the driving force for grid growth, the arsenic addition strongly suppresses creep deformation in low-antimony alloys and results in a reduced mobility for the grid-growth process. Since the rate of a kinetic process is determined by the product of the driving force and mobility, the overall effect of the arsenic addition is to reduce the growth rate. It is of interest to note that the creep rate ($\dot{\varepsilon}$ in Eq. (1)) was approximately proportional to $\exp(-12C_{As})$, and that the growth term, $G$, was proportional to $\exp(-4C_{As})$. Based on the universal rate equation, the rate of a kinetic process is equal to the product of the driving force and mobility. It can be concluded that the corrosion-induced driving force for growth must be proportional to $\exp(8C_{As})$.

The strong effect of arsenic in suppressing the creep deformation is due to its effect on precipitation in low-antimony–lead alloys. Using TEM, Borchers and Reuleaux [18] found that antimony in a Pb–2wt.%Sb alloy precipitated out in room-temperature ageing as rod-like particles with an average length of 150 nm. On the other hand, antimony in a Pb–2wt.%Sb–0.1wt.%As alloy precipitated out as coherent spherical particles with an average diameter of 15 nm. After being aged naturally for two days, the precipitates were still coherent and the size grew to 30 nm. Tsumuraya and Nishikawa [19] explored the mechanism of precipitation acceleration by arsenic addition. They found that the binding energy of arsenic atoms with quenching-in vacancies was much higher than their antimony counterparts. Consequently, arsenic additions increase the vacancy concentration in a quenched alloy. Antimony precipitation was found to be a three-stage process. The excess vacancy concentration enhances the diffusion of arsenic and antimony atoms, which facilitates the formation of an intermediate phase with an apparent formula of AsSb. Spherical antimony particles grow on such cores and become the equilibrium phase.

Precipitates are heterogeneous sites in an alloy, which impede dislocation motion in deformation and enhance chem-

ical reaction in corrosion. Arsenic released from grids due to corrosion is known, however, to be incorporated in the active material and has been found to be beneficial for restoration of the active-mass structure partly damaged during discharging [20]. Arsenic at up to 0.2 wt.% has also been found [20] to have a strong effect on the maintenance of electrode capacity although a further increase in arsenic content to 0.8 wt.% had only a slight influence. As mentioned earlier, the effect of arsenic on the creep resistance of the alloy reached a limit at an arsenic content of about 0.2 wt.%; further increase in arsenic content resulted in deterioration of the creep resistance of the alloy. Combining the findings available in the open literature with those obtained in the present study, it can be concluded that arsenic addition up to 0.2 wt.% is beneficial for the mechanical strength and the overall electrochemical performance of low-antimony–lead grid alloys.

## 6. Conclusions

1. Lead grid alloys with wide solidification ranges can be readily cast using Cominco's Multi-Alloy Caster™ due to the high cooling rate realized by the melt-drag process.
2. The overall performance of low-antimony–lead alloys is strongly affected by their arsenic content. In spite of enhanced corrosion, arsenic up to 0.2 wt.% is beneficial to mechanical strength, growth resistance, and deep-cycling capacity retention.
3. Weight losses of low-antimony–lead alloys in potentiostatic corrosion tests are proportional to antimony equivalent, defined as $(C_{Sb} + 10.2C_{As})$.
4. The microstructure and properties of a Pb–Ca–Sn alloy are strongly determined by its Sn:Ca ratio.

## Acknowledgements

The authors wish to thank Mr M.J. Dewar for carrying out the electrochemical tests. The authors are also grateful to Cominco Ltd., Product Technology Centre, for permission to publish this work.

## References

[1] H. Niklas, Grain refining technique for lead battery alloys with selenium, *Proc. Int. Symp. Industrial Uses of Selenium and Tellurium, Toronto, Canada, 21–23 Apr. 1980*, pp. 244–253.
[2] M. Abdel-Reihim, N. Hess, W. Reif and M.E.J. Birch, *J. Mater. Sci., 22* (1987) 213–218.
[3] U. Heubner, I. Mueller and A. Ueberschaer, *Z. Metallk., 66* (1975) 74–79.
[4] P. Rao, *US Patent No. 5 298 350* (29 Mar. 1994).
[5] F.N. Coady, Cooling curves for lead–silver alloy, *File No. 623-003, Internal Memorandum*, Cominco, Ltd., Product Technology Centre, Apr. 1992.
[6] J.G. Larson, personal communication, GNB Inc., 1992.
[7] *Can. Patent Applic. No. 155–736* (1973).
[8] M. Myers, *The Battery Man*, (Sept.) (1987) 24.
[9] J. Devitt and M. Myers, *J. Electrochem. Soc., 128* (1981) 1641.
[10] Y. Watanabe, Y. Suzuki, Y. Nagata and K. Hoshino, *US Patent No. 4 498 519* (12 Feb. 1985).
[11] J. Sklarchuk, M.J. Dewar, E.M. Valeriote and A.M. Vincze, *J. Power Sources, 42* (1993) 47–53.
[12] N.-Y. Tang and E.M. Valeriote, Growth of expanded antimonial lead alloy battery grids, *J. Electrochem. Soc., 142* (1995) 2144–2148.
[13] R.C. Percy, *PTC Project 71-5-626, Rep. Nos. 1, 2 and 3*, Cominco, Ltd., Mississauga, Ont., Canada, 1973.
[14] D. Kelly and P. Niessen, *Met. Sci., 18* (1984) 467–470.
[15] L. Bouirden, J.P. Hilger and J. Hertz, *J. Power Sources, 33* (1991) 27–50.
[16] D. Kelly, *Ph.D. Thesis*, University of Waterloo, Ont., Canada, 1985.
[17] H. Giess, *J. Power Sources, 53* (1995) 31–43.
[18] H. Borchers and M. Reuleaux, *Metall, 35* (1981) 878–882.
[19] K. Tsumuraya and S. Nishikawa, *Metall. Trans. A, 11* (1980) 949–954.
[20] D. Pavlov, A. Dakhouche and T. Rogachev, *J. Power Sources, 30* (1990) 117–129.